TOMISŁAW GOŁĘBIOWSKI*

INTRODUCTION TO NUMERICAL MODELING OF ELECTROMAGNETIC WAVE FIELD ON THE EXAMPLE OF GEORADAR DATA RECORDED IN RIVER DIKE

WPROWADZENIE DO MODELOWANIA NUMERYCZNEGO ELEKTROMAGNETYCZNEGO POLA FALOWEGO NA PRZYKŁADZIE BADAŃ GEORADAROWYCH PRZEPROWADZONYCH NA WALE PRZECIWPOWODZIOWYM

Abstract

Selected result of GPR surveys, which were carried out on the dike of the Vistula River, three days after the flood in 2010, was presented in the paper. Radargram was processed in a standard way, which allowed 2D visualization of main loose zones in the examined dike. Theoretical background of numerical modelling of electromagnetic wave field in the geological medium was presented in the paper. The results of numerical modelling were used for the evaluation of water and air saturation of loose zones during radargram interpretations.

Keywords: georadar, numerical modelling, river dike

Streszczenie

W artykule przedstawiono wybrany wynik z badań georadarowych wału wiślanego, które przeprowadzono trzy dni po powodzi w 2010 roku. Echogram poddano standardowemu przetwarzaniu, co pozwoliło na wizualizację 2D rozkładu głównych stref rozluźnień w badanym wale. W artykule zamieszczono podstawy teoretyczne modelowania numerycznego rozkładu pola elektromagnetycznego w ośrodku geologicznym. Na etapie interpretacji echogramu wykorzystano wyniki modelowania w celu określenia nasycenia rozluźnień wodą i powietrzem.

Słowa kluczowe: georadar, modelowanie numeryczne, wały przeciwpowodziowe

* Prof. DSc. PhD. Tomisław Gołębiowski, Department of Geotechnics, Faculty of Environmental Engineering, Cracow University of Technology

1. Introduction

Application of geophysical methods for the examination of technical conditions of river dikes is not a new matter. For years, for this purpose, selected methods were used, first of all: electrical methods [1– 4], georadar surveys [5–10], electromagnetic profiling [1–3], seismic surveys [1, 2, 11–13]. Unfortunately, despite long lasting tradition of using different geophysical methods for dike examination, the results of measurements are often difficult for unequivocal interpretation. It is caused by few facts, among others:

a) several looseness are small and their dimensions are on the boundary of the detection ability of geophysical methods,

b) loose zones, in the body of dike, are distributed randomly, therefore, it is difficult to prepare a proper interpretative model,

c) physical properties of looseness are depending on the amount of water, clay and air in the porous space, but the amount of these media is unknown during surveys.

The author focused, in the paper, on the analysis of abilities and limitations of the georadar method (GPR) for loose zones detection in the dike. Among different GPR measurement techniques, the most popular is short or zero offset reflection profiling, and therefore, such technique will be analysed in the paper.

GPR surveys were carried out on the Vistula river dike in Cracow (Fig. 1A), 3 days after the flood in 2010, when water declined to the basement of the dike (Fig. 1B). Georadar profile was designed in the middle of the top part of the dike, where no under- and over-ground interferences occurred in surrounding of the profile (Fig. 1C).

Geological information (Fig. 2A) obtained from the borehole WL-11 (Fig. 1C) depicted that the body of the dike was formed by sand and clayey sand, so attenuation of electromagnetic wave should not be very high (Table 1) and the GPR method should allow to examine the whole body of the dike up to the basement, i.e. to depth ca. 2.3 m (Fig. 2A).

It is assumed [14] that if the following criteria are met, i.e.:

– wetness $W_n > 19\%$,

– density $\rho < 1.70$ t/m3,

– compaction factor $I_s < 0.92$,

the examined dike is in bad technical condition. The results of laboratory tests, carried out on the ground samples no. 1 and no. 2 (Fig. 2A), allow to assume that the whole dike in the investigation site is in a very bad technical condition. Also, the result of diving rod sounding (Fig. 2B) confirms a bad technical condition of the examined dike and undersoil to a depth of 4 m.

The aim of the GPR surveys was the two-dimensional (2D) visualization of loose zones distribution, detected formerly by borehole and geotechnical sounding.

GPR measurements were performed using the ProEx system (MALA Geoscience, Sweden) with 500 MHz shielded antenna with max. depth penetration of ca. 5m and mean resolution of ca. 0.05 m. Traces were recorded every 0.025m and for every one trace assumed 512 samples and sampling frequency was equal to 5000 MHz; stacking 32 times was defined during data acquisition for improvement of signal-to-noise ratio.

Radargram after standard processing in ReflexW program (SandmeierGEO, Germany) was presented in Fig. 3; the following processing procedures were used [15, 16]: t_0 correction, dewow function, DC correction, Butterworth filtering, 1D median filtering, gain function, background removal, stacking, 2D averaging filtering, Stolt migration. For better visualisation,

non-equal scales of vertical and horizontal axes were applied and amplitudes of reflections were normalised to the max. amplitude of the direct air wave. For the time-depth conversion, mean velocity $v = 0.085$ m/ns was assumed on the basis of diffraction hyperbolas analysis.

In radargram presented in Fig. 3, randomly distributed anomalies, i.e. high amplitude reflections (with red and black colours), are easily noticed. GPR anomalies may be correlated with the loose zones. The result of GPR surveys correlated well with information obtained from the borehole and geotechnical sounding and it may be assumed that the whole body of the examined dike is in bad technical condition. Analysing Fig. 3, it may be observed that more high amplitude reflections are located in the first (left) part of radargram, thus this part of the dike may be assumed as more intensively disintegrated.
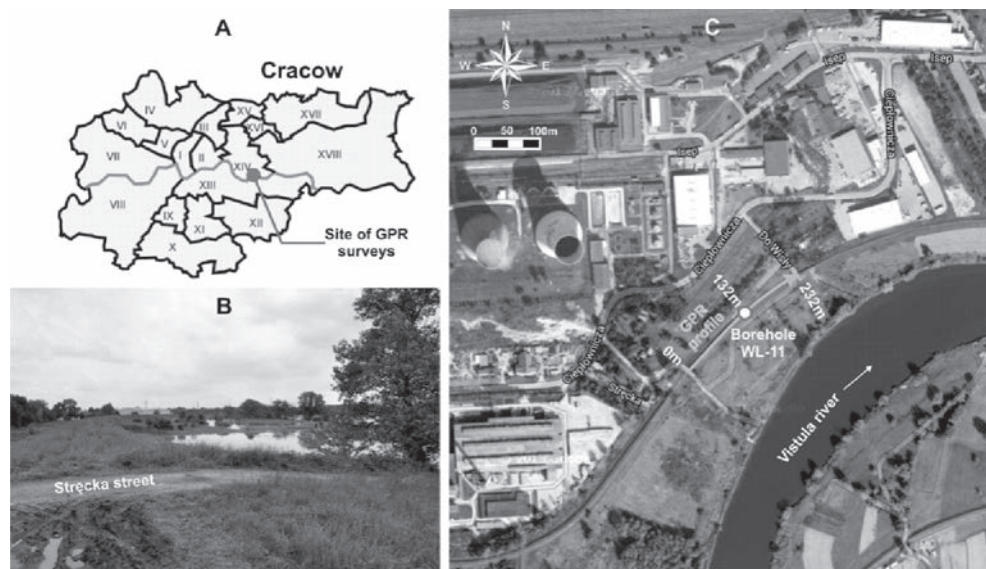

Fig. 1. A) Site of GPR surveys on the dike of the Vistula River in Cracow; B) Investigation site 3 days after the flood in 2010; C) Location of GPR profile and borehole on the top of the dike (base map: www.google.pl/maps)
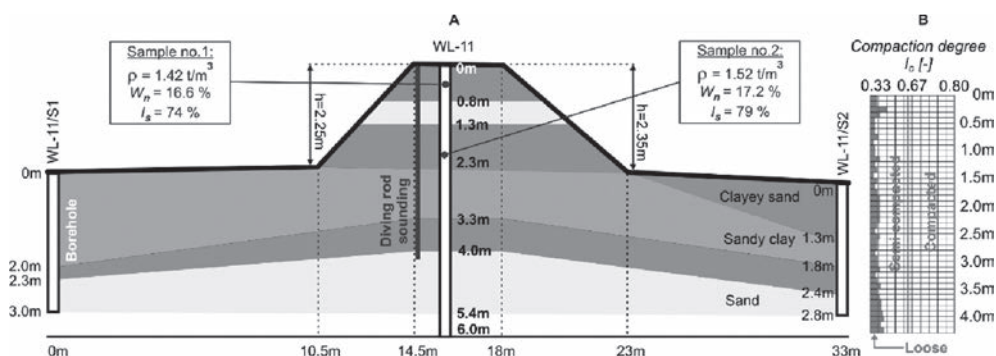

Fig. 2. A) Geological and laboratory data from borehole WL-11; B) Result of diving rod sounding
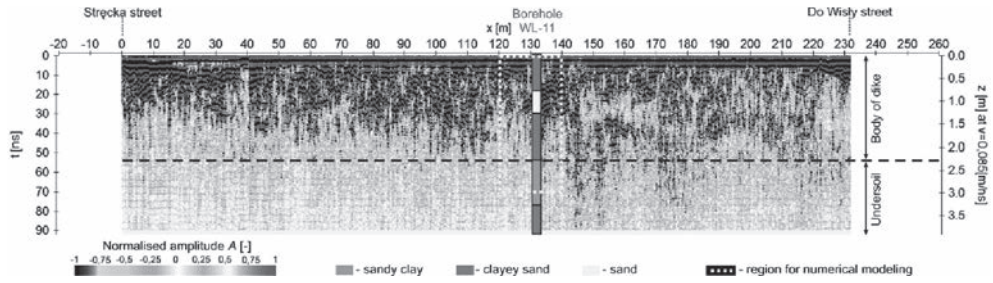
Fig. 3. Radargram after standard processing

Standard, i.e. visual, analysis of radargram allows only to draw conclusions presented in previous sentence, so only qualitative interpretation is possible. Application of numerical modelling for radargram interpretation allows to draw further conclusions, which will be presented in chapter 3.

2. Theoretical background of numerical modelling of electromagnetic wave for GPR method

The most popular technique of modelling of an electromagnetic wave field is the FDTD (*Finite Difference Time Domain*) technique [17], and this technique is commonly used for the GPR method [18–21]. Detailed information about the application of the FDTD technique for radargram interpretation may be found in above-mentioned publications and in the following part of the paper, only basic information will be presented.

In order to solve Maxwell equations (1)–(4) with the use of FDTD technique, the discretization of continuous geological model is needed.

$$\nabla \cdot \vec{E} = 0 \tag{1}$$

$$\nabla \cdot \vec{H} = 0 \tag{2}$$

$$\nabla \times \vec{E} = -\mu \cdot \frac{\partial \vec{H}}{\partial t} \tag{3}$$

$$\nabla \cdot \vec{E} = 0 \quad \nabla \cdot \vec{H} = 0 \quad \nabla \times \vec{E} = -\mu \cdot \frac{\partial \vec{H}}{\partial t} \quad \nabla \times \vec{H} = \sigma \cdot \vec{E} + \varepsilon \cdot \frac{\partial \vec{E}}{\partial t} \tag{4}$$

where:
∇ — nabla operator,
$\vec{E}$ [V/m] — electric component of electromagnetic field,
H [A/m] — magnetic component of electromagnetic field,
μ [H/m] — magnetic permittivity,

t [s]　　　– time,
σ [S]　　　– electrical conductivity,
ε [F/m]　　– electrical permittivity.

In discrete model, the components of electromagnetic wave field are defined only in the grid points (Fig. 4A) and numerical analysis is conducted with the assumption that electromagnetic wave is the TEM (Transverse Electromagnetic) wave (Fig. 4B).
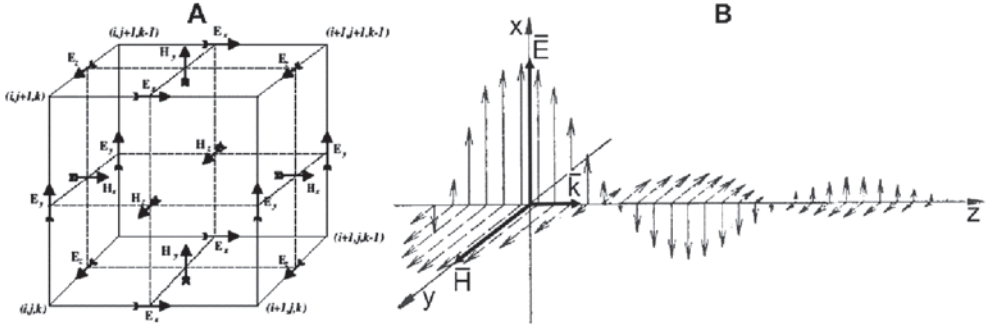

Fig. 4. A) A grid zone for solving of Maxwell equations with the use of FDTD technique (www. gprmax.com); B) Transverse Electromagnetic wave

The following notation may be introduced for the FDTD technique for 3D modelling:
− $\Delta x, \Delta y, \Delta z$ – dimensions of grid zones in x, y and z directions,
− i, j, k – numbering of grid points in x, y and z directions,
− Δt – dimension of time step,
− n – number of time step.

Discrete form of Maxwell equations for the FDTD technique is as follow [22]:

$$E_x^{n+1}(i,j,k) \approx\sim K_x(j,j,k)E_x^n(i,j,k)+$$
$$+P_x\left[\frac{H_z^{n+1/2}(i,j+1,k)-H_z^{n+1/2}(i,j,k)}{\Delta y} - \frac{H_y^{n+1/2}(i,j,k+1)-H_y^{n+1/2}(i,j,k)}{\Delta z}\right] \quad (5)$$

$$E_y^{n+1}(i,j,k) \approx\sim K_y(j,j,k)E_y^n(i,j,k)+$$
$$+P_y\left[\frac{H_z^{n+1/2}(i,j,k+1)-H_z^{n+1/2}(i,j,k)}{\Delta y} - \frac{H_y^{n+1/2}(i+1,j,k)-H_z^{n+1/2}(i,j,k)}{\Delta z}\right] \quad (6)$$

$$E_z^{n+1}(i,j,k) \approx\sim K_z(j,j,k)E_z^n(i,j,k)+$$
$$+P_z\left[\frac{H_y^{n+1/2}(i+1,j,k)-H_y^{n+1/2}(i,j,k)}{\Delta x} - \frac{H_x^{n+1/2}(i,j+1,k)-H_x^{n+1/2}(i,j,k)}{\Delta y}\right] \quad (7)$$

$$H_x^{n+1/2}(i,j,k) \approx H_x^{n+1/2} + \frac{\Delta t}{\mu_x(i,j,k)}$$

$$\left[\frac{E_y^n(i,j,k+1) - E_y^n(i,j,k)}{\Delta z} - \frac{E_y^n(i,j+1,k) - E_y^n(i,j,k)}{\Delta y} \right] \tag{8}$$

$$H_y^{n+1/2}(i,j,k) \approx H_y^{n+1/2} + \frac{\Delta t}{\mu_y(i,j,k)}$$

$$\left[\frac{E_z^n(1+i,j,k) - E_z^n(i,j,k)}{\Delta x} - \frac{E_x^n(i,j,k+1) - E_x^n(i,j,k)}{\Delta z} \right] \tag{9}$$

$$H_z^{n+1/2}(i,j,k) \approx H_z^{n+1/2} + \frac{\Delta t}{\mu_z(i,j,k)}$$

$$\left[\frac{E_x^n(i,j+1,k) - E_x^n(i,j,k)}{\Delta y} - \frac{E_y^n(1+i,j,k) - E_y^n(i,j,k)}{\Delta x} \right] \tag{10}$$

where parameters K and P describe material properties of the analysed medium, i.e.:

$$K_{x,y,z}(i,j,k) = \frac{\varepsilon_{x,y,z}(i,j,k) - 0.5\Delta t \sigma_{x,y,z}(i,j,k)}{\varepsilon_{x,y,z}(i,j,k) + 0.5\Delta t \sigma_{x,y,z}(i,j,k)} \tag{11}$$

$$P_{x,y,z}(i,j,k) = \frac{\Delta t}{\varepsilon_{x,y,z}(i,j,k) + 0.5\Delta t \sigma_{x,y,z}(i,j,k)} \tag{12}$$

Usually, in algorithms for numerical modelling of GPR wave field material properties of analysed geological media are defined as follow:
– value of electrical conductivity σ [S] is defined in unit of [S/m],
– instead of electrical permittivity ε [F/m], value of relative dielectric constant ε_r [–] is defined, according the formula (13),
– instead of magnetic permittivity μ [H/m], value of relative magnetic permittivity μ_r [–] is defined, according the formula (14); for geological media, a constant value of μ_r, equals 1 (like for vacuum) is assumed for modelling.

$$\varepsilon_r = \frac{\varepsilon}{\varepsilon_0} \varepsilon_0 = 8.85 \cdot 10^{-12} \, [\text{F/m}] \tag{13}$$

$$\mu_r = \frac{\mu}{\mu_0} \mu_0 = 4.5 \cdot 10^{-7} \, [\text{H/m}] \tag{14}$$

where: ε_o and μ_0 – adequately electrical and magnetic permittivity of vacuum.

For convergence and stability of numerical solution, two criteria (15), (16) have to be met, i.e. referred to max. dimension of grid zone Δ (i.e. Δx and Δy and Δz) and max. time step Δt.

$$\Delta \leq \frac{\lambda}{10} \tag{15}$$

$$\Delta t = \frac{1}{v \cdot \sqrt{\frac{1}{(\Delta x)^2} + \frac{1}{(\Delta y)^2} + \frac{1}{(\Delta z)^2}}} \tag{16}$$

where: λ [m] – wave length, v [m/s] – velocity of propagation of electromagnetic wave.

Velocity in equation (16) as well as attenuation of modelled medium α [dB/m] may be described by the following formulae:

$$v = \frac{c}{\sqrt{\left(\frac{\varepsilon\mu}{2}\right) \cdot \left(\left(1 + \frac{\sigma}{\omega\varepsilon}\right)^2 + 1\right)}} \tag{17}$$

$$\alpha = \omega \sqrt{\left(\frac{\varepsilon\mu}{2}\right) \cdot \left(\sqrt{1 + \left(\frac{\sigma}{\omega\varepsilon}\right)^2} - 1\right)} \tag{18}$$

where: c [m/s] – velocity of electromagnetic wave in vacuum ($3 \cdot 10^8$ m/s), ω [rad/s] – angular frequency.

On the upper boundary of the numerical model, a strip with material properties of air, i.e. $\varepsilon_r = 1$, $\mu_r = 1$, $\sigma = 0$ mS/m, is introduced. In the left, right and bottom boundaries of numerical model, the absorbing boundary condition is defined by increasing of attenuation (18) in the boundary area.

For excitation of propagation of the electromagnetic wave in the numerical model, a source, which simulates emission of wave from transmitter antenna, has to be defined. Proper definition of the source in modelling is a complicated problem, so only the main stages of the source construction will be described. At the first stage of source constriction, the type of source has to be defined, e.g. plane wave, point source, exploding reflector [16]. At the next stage, the orientation of transmitter and receiver antennae have to be defined [23, 24]. At the last stage, adequate source function (i.e. signal) for controlling of source has to be defined [16], e.g. Ricker, sinus, Kuepper signal or real signal adequately discretised from radargram.

In the paper, only the reflection technique is analysed, so only basic information about the reflection of the electromagnetic wave is presented in the following part of this chapter. The reflection of the electromagnetic wave is observed on the geological boundary or anthropogenic underground objects when difference of impedances Z (19) appears in the

46

geological medium. Two different situations (Fig. 5) may occur when the front of wave reaches the geological boundary.

$$Z = \sqrt{\frac{j\omega\mu}{\sigma + j\omega\varepsilon}} \tag{19}$$

where: j – imaginary unit.
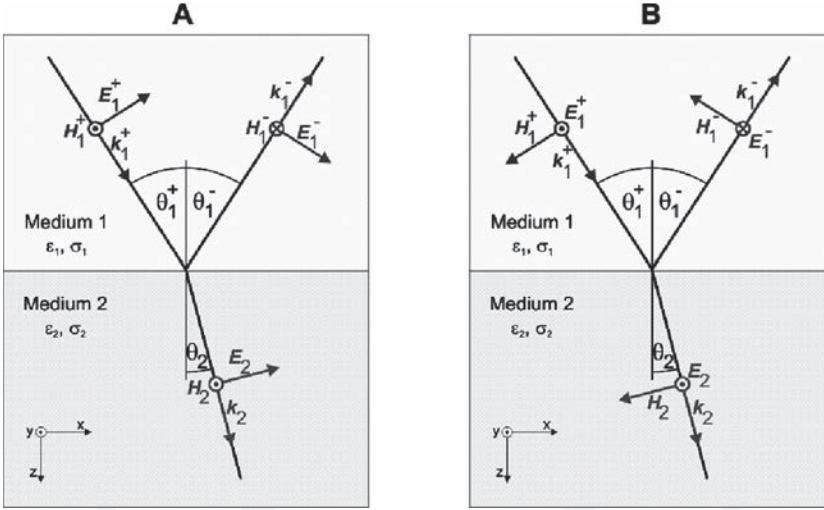

Fig. 5. Schemes for analysing of wave reflection for: A) perpendicular polarised wave ($\perp$), B) parallel polarised wave ($\parallel$)

Reflection R and transmission T coefficients for both situations presented in Fig. 5 are as follow:

$$R_{\parallel} = \frac{Z_2 \cdot \cos\theta_2 - Z_1 \cdot \cos\theta_1}{Z_2 \cdot \cos\theta_2 + Z_1 \cdot \cos\theta_1} \tag{20}$$

$$R_{\perp} = \frac{Z_2 \cdot \cos\theta_1 - Z_1 \cdot \cos\theta_2}{Z_2 \cdot \cos\theta_1 + Z_1 \cdot \cos\theta_2} \tag{21}$$

$$T_{\parallel} = \frac{2Z_2 \cdot \cos\theta_1}{Z_1 \cdot \cos\theta_1 + Z_2 \cdot \cos\theta_2} \tag{22}$$

$$T_{\perp} = \frac{2Z_2 \cdot \cos\theta_1}{Z_2 \cdot \cos\theta_1 + Z_1 \cdot \cos\theta_2} \tag{23}$$

Scheme of reflection of electromagnetic wave, presented in Fig. 5, is valid only for simple situations, e.g. horizontal geological boundary or underground object with simple shape. In real conditions, geological structures are usually complicated, furthermore, heterogeneity and anisotropy often appear in the geological medium and objects with complicated shapes may occur in the geological medium. In the described real situations, a mathematical analysis of the process of propagation and the reflection of the electromagnetic wave is very difficult, and thus, the only solution is delivered by numerical modelling.

3. The results of modelling

When loose zones occur in a dike, two different situations have to be analysed, i.e.:
– presence of the so-called "dry looseness" i.e. looseness without direct hydraulic connectivity with the surface of a dike; in such a situation, loose zones are filled mainly with air; an example of such type of looseness are channels made by moles and voles;
– presence of the so-called "wet looseness"; in such a situation, presence of hydraulic connectivity between several looseness and surface of dike cause that different amount of air and/or water may appear in the looseness, depending of time of water supply from precipitation or from river (during the flood).

The second situation, described above, is more dangerous during the flood because the presence of hydraulic connectivity among several looseness causes movement of water inside of the dike, washing out of material and, in consequence, breaking of the dike. Therefore, the aim of numerical modelling was the answer to the question whether loose zones, in the investigated dike, were water saturated or not.

On the basis of geological information from borehole WL-11 (Fig. 2A), two-dimensional numerical models were constructed (Fig. 6); geotechnical data (Fig. 2B) delivered information that the body of the dike was equally disintegrated between top and basement of dike, which was presented in numerical models by equally distributed looseness (Fig. 6). Vertical dimensions of models (i.e. 2.3m) referred to the height of the examined dike (Fig. 2A); horizontal dimensions (i.e. 20 m) were adequate to the region around borehole WL-11 (Fig. 3 – yellow rectangle).
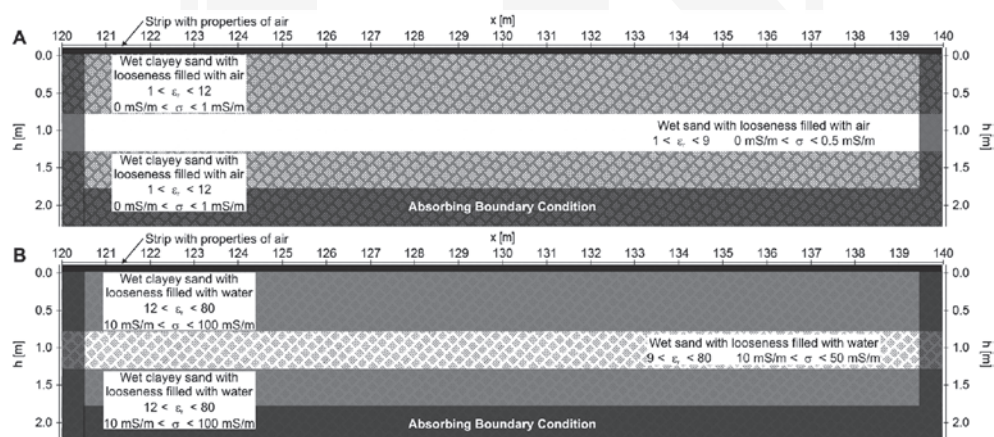

Fig. 6. Numerical models for analysis of looseness saturation with air (A) and water (B)

A strip, which simulates air, was inserted on the upper boundary of models; and on the other boundaries, absorbing boundary condition was defined (Fig. 6).

Models were discretised by a grid with dimensions $\Delta x = \Delta h = 0.01$m and time step $\Delta t = 0.01$ ns was assumed according to the formulae (15, 16). Solving was carried out in time window $T = 90$ ns according to time window assumed during terrain surveys (Fig. 3).

The source of electromagnetic wave was defined as so-called "exploding reflector" and the source function, with central frequency 500 MHz, was assumed on the basis of discretisation of real signal taken from radargram. In source and registration points, Ey component of electromagnetic wave field was taken into account adequately to geometry of transmitter and receiver antennae used during terrain surveys.

The most difficult stage of models preparation was the proper construction of loose zones, which had random distribution in the dike (Fig. 7A). There is no possibility to describe the dimensions of several looseness and their distribution in space (Fig. 7A) in a deterministic way. It is also impossible to define the amount of water and/or air in porous spaces of the dike deterministically, so it is impossible to deliver equivalent material properties of mixture of sand (quartz), clay, water and air (Fig. 7B). In such situation, the only technique of construction of loose zones in numerical models seems to be an application of stochastical model. Detailed description of the application of stochastical models in interpretation of georadar data was presented in book [9], but in following part of this chapter, only basic information is presented.
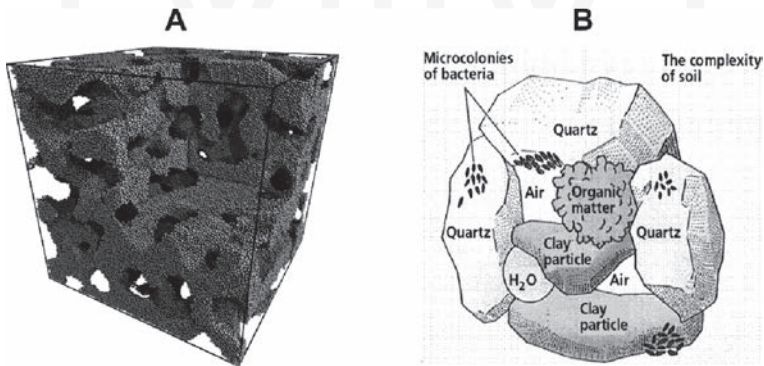

Fig. 7. A) Random distribution of loose zones in dike (www.utdallas.edu); B) Complexity of analysed medium (secretsofsoil.com)

A random generator was applied for construction of stochastical model. In the first step, „i" and „j" addresses of grid point were randomly chosen on the basis of self-similar distribution. In the second step, randomly chosen grid point assigned equivalent values of ε_r and σ (Table 1) using random generator with application of Gauss distribution, i.e.:

– for air-filled looseness (Fig. 6A), it was assumed that the values of ε_r changed randomly from 1 (value for air) to 12 (value for wet mixture of sand and clay) and σ changed randomly from 0 mS/m (air) to 10 mS/m (wet sand and clay),

– for water-filled looseness (Fig. 6B), it was assumed that the values of ε_r changed randomly from 12 (wet sand and clay) to 80 (value for water) and σ changed randomly from 10 mS/m (wet sand and clay) to 100 mS/m (looseness filled with water and clay minerals after the flood).

Value $\varepsilon_r = 12$, assumed for wet mixture of sand and clay, is adequate to the velocity $v = 0.085$ m/ns determined from radargram on the basis of diffraction hyperbola analysis. For all grid points, constant value of μ_r equals 1 was assumed. In the next step, second grid point was randomly chosen, and randomly chosen values of ε_r and σ were assigned to this grid point. This procedure was carried out as long as all grid points had assigned material properties.

The results of modelling, i.e. synthetic radargrams, for both analysed models shown in Fig. 8C,D; synthetic radargrams, were presented in the form of envelopes counted from Hilbert transform [16]. For comparison, measured radargram in form of amplitudes distribution (Fig. 8A) and in form of envelopes (Fig. 8B) were presented.

T a b l e 1

Material properties of analysed media [25]

Medium	Relative dielectric constant ε_r [−]	Relative magnetic permittivity μ_r [-]	Electrical conductivity σ [mS/m]	Velocity of electromagnetic wave v [m/ns]	Attenuation α [dB/m]
Fresh water	80	1	0.5	0.03	0.1
Air	1	1	0	0.3	0
Sand (dry - water saturated)	3 – 30	1	0.01 – 1	0.17 – 0.05	0.01 – 0.3
Clay (dry - water saturated)	5 – 40	1	2 – 1000	0.13 – 0.05	1 – 300

During analysis of looseness filling (i.e. water and air), the parameters discussed below should be taken into account.

Velocity v of electromagnetic wave is higher in air-saturated looseness ($v_{air} = 0.3$ m/ns) than in water-saturated looseness ($v_{water} = 0.03$ m/ns) – Table 1; these facts might be used in an interpretation if a geological boundary would be recorded under the loose zone, e.g. a boundary between clayey sand and sand in analysed situation (Fig. 2A). Air-filling of looseness caused that reflections from this boundary appeared in radargram in lower times (due to higher velocity in air) than in region without looseness. When loose zones are filled with water, which characterises itself by low velocity, reflections from geological boundary appear in higher times in radargram. Unfortunately, no reflections from boundary between clayey sand and sand were recorded, so there was no possibility to analyses changes of velocity of electromagnetic wave in loose zones.

Reflection coefficient R in boundary between wet ground and water-filled looseness is lower ($R = -0.4$) than in air-filled looseness ($R = 0.6$); the mentioned fact is easily noticed in Fig. 8C,D were in Fig. 8C more high amplitude reflections were recorded than in Fig. 8D. Comparing result depicted in Fig. 8B (measured radargram) and Fig. 8C,D (synthetic radargrams), it might be assumed that distribution of reflections in Fig. 8B is similar to Fig. 8D; such observation allows drawing the conclusion that, in the analysed part of the dike, looseness were filled with water.

Polarisation of reflections origin from water-saturated looseness is opposite to polarisation of source signal; when looseness are filled with air, a polarisation of reflections is the same as in source signal. When well-separated looseness or voids occur in the investigated medium, polarisation becomes a very good indicator of looseness filling; in analysed situation (Fig. 8A) reflections are overlaid, so polarisation is not useful tool for analysis of looseness filling.

Loose zones, filled with different amount of water and clay (e.g. after the flood), have higher **attenuation** (Table 1) than air-saturated looseness; this fact causes that amplitudes of reflections are highly decreased is certain sub-region of analysed medium. The mentioned effect may be observed in Fig. 8B and Fig. 8D, which allow to draw the conclusion that looseness were filled with water in the analysed part of the dike. On the contrary, presence of air in looseness caused better propagation of wave, and thus, stronger reflections from deeper parts of the dike might be recorded (Fig. 8C).

Resolution of GPR method, which is a function of wave frequency and velocity, is higher in water-saturated medium (Fig. 8D) than in dry one (Fig. 8C). High resolution observed in radargram presented in Fig. 8B depicts that loose zones were water-saturated during the surveys; possibility of outlining of several sub-regions in loose zone is similar in Fig. 8B and Fig. 8D, which confirms interpretation presented in previous sentence.
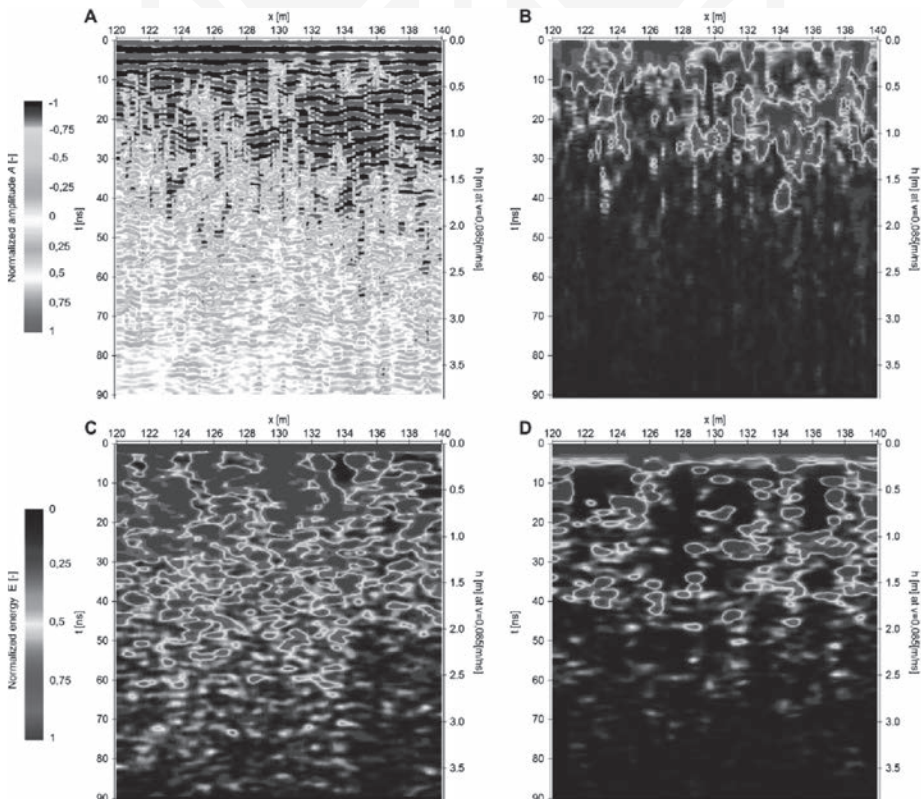

Fig. 8. Part of measured radargram around borehole WL-11 in form of amplitude distribution (A) and in form of envelopes (B); synthetic radargrams in form of envelopes with looseness filled with air (C) and water (D)

In the situation analysed in the paper, only three from five parameters might be taken into account. However, these parameters delivered information that loose zones were water-saturated, so a hydraulic connectivity was present in the examined dike.

Geological (Fig. 2A) and geotechnical (Fig. 2B) data delivered information that the whole body of the dike was highly disintegrated in point WL-11. Geophysical data (Fig. 3) showed that a large part of the dike around point WL-11 is disintegrated. The results of modelling depicted that there was a possibility of water migration within loose zones of the examined dike. All above-listed information show that the investigated part of the dike should be renovated immediately.

4. Conclusions

Contrary to geological or geotechnical surveys, geophysical methods deliver continuous information about loose zones distribution in the examined medium. These methods are faster, cheaper and non-invasive in comparison with drilling and sounding. Standard analysis of geophysical data allows only for qualitative interpretation, so in analysed situation, only outlining the loose zones in the dike was possible. Application of numerical modelling in interpretation allows, in certain situations, to carry out a detailed interpretation of measured data. In analysed situation, synthetic radargrams allow to draw the conclusion that looseness were water-saturated. In order to decrease ambiguity of interpretation, the results of geophysical measurements and numerical modelling have to be correlated with the results of geological or geotechnical surveys. This would allow to deliver information about amount of water in loose zones.

References

[1] Niederleithinger E., Weller A., Lewis R., Stotzner U., Fechner T., Lorenz B., Nießen J., *Evaluation of Geophysical Methods for River Embankment Investigation*, Report of project "Deistrukt", Germany 2005.
[2] Inazaki T., Sakamoto T., *Geotechnical Characterization of Levee by Integrated Geophysical Surveying*, Proceedings of International Symposium on Dam Safety and Detection of Hidden Troubles of Dams and Dikes, Xi'an 2005.
[3] Asch T.H., Deszcz-Pan M., Burton B.L., Ball L.B., *Geophysical Characterization of the American River Levees using Electromagnetics, Capacitively Coupled Resistivity and DC Resistivity*, Open-File Report no. 2008–1109, U.S. Geological Survey, Reston, Virginia 2008.

52

[4] Golebiowski T., Tomecka-Suchon S., Farbisz J., *Using of Complex Geophysical Methods for Non-invasive Examination of the River Embankments*, Proceedings of European Symposium on "Problems of flood defense", Org. SITPF and NOT, Paris (in Polish) 2012.

[5] Prinzio M., Bittelli M., Castellarin A., Pisa P.R., *Application of GPR to the Monitoring of River Embankments*, Journal of Applied Geophysics, vol. 71, iss. 2–3, 2010.

[6] Marcak H., Golebiowski T., Tomecka-Suchon S., *Analysis of Possibility of Using of GPR Refraction Waves for Detection of Changes in River Embankments*, Quarterly AGH-UST Geology, vol. 31, iss. 3–4 (in Polish) 2005.

[7] Golebiowski T., *Changeable-offset GPR Profiling for Loose Zones Detection in Levees*, Proceedings of International Conference "Near Surface 2008", EAEG Org., Cracow 2008.

[8] Golebiowski T., *Velocity Analysis in the GPR Method for Loose Zones Detection in River Embankments*. Proceedings of International Conference "GPR 2010", Org. International Association of GPR, Lecce, Italy, 2010.

[9] Golebiowski T., *Application of the GPR Method for Detection and Monitoring of Objects with Stochastical Distribution in the Geological Medium*, Dissertation no. 251, AGH University of Science and Technology Press, Krakow (in Polish) 2012.

[10] Marcak H., Golebiowski T., *The Use of GPR Attributes to Map a Weak Zone in a River Dike*, Exploration Geophysics, 45(2), CSIRO Publishing, Collingwood 2014.

[11] Pilecki Z., *Recognising of Dike Undersoil Using of Seismic Method*. Monthly of WUG, 5 (117), Katowice (in Polish) 2004.

[12] Pilecki Z., Kłosiński J., *Evaluation of Technical Condition of Dike Using of Seismic Method,* Monthly of WUG, 6 (130), Katowice (in Polish) 2005.

[13] Chen Ch., Liu J., Xia J., Li Z., *Integrated Geophysical Techniques in Detecting Hidden Dangers in River Embankments*, Journal of Environmental and Engineering Geophysics, vol. 11, no. 2, 2006.

[14] Wilun Z., *Basis of Geotechnics*, KiL Ed., Warsaw (in Polish), 2000.

[15] Annan A.P., *Practical Processing of GPR Data*, Sensor and Software Inc., Canada 1999.

[16] ReflexW, *User Guide of ReflexW computer program*, SandmeierGeo firm, Karlsruhe 2014.

[17] Yee K.S., *Numerical Solution of Initial Boundary Value Problems Involving Maxwell's Equations in Isotropic Media*, IEEE Trans. Antenna. Propagation, no. 14, 1966.

[18] Golebiowski T., *Numerical Modeling of GPR Wave Field Using of FDTD Technique*, Geoinformatica Polonica, no. 8, Cracow (in Polish) 2006.

[19] Golebiowski T., *Application of Numerical Modelling of Georadar Wave Filed for Investigation of Hydrocarbon Contaminated Ground*, Ph.D. dissartation, AGH-UST, Cracow (in Polish) 2005.

[20] Golebiowski T., *Introduction to Interpretation of GPR Date Using of Numerical Modelling*, Polish Geological Review, vol. 52, no. 7, Warsaw (in Polish) 2004.

[21] Marcak H., Gołębiowski T., *Computer Simulation of Hydrocarbon Flow and Wave Field for Interpretation GPR Measurements in Contaminated Sites*, Proceedings of International Conference "SAGEEP 2005", EEGS Org., Atlanta 2005.

[22] Fornberg B., *Some Numerical Techniques for Maxwell's Equations in Different Types of Geometries*, University of Colorado, Department of Applied Mathematics, Boulder 2002.

[23] Marcak H., Golebiowski T., *Analysis of Detection Possibility of GPR Technique for Changeable Geometry of Antennae*. Proceedings of Conference on "Geophysics in Geology and Mining", vol. dedicated to prof. W.M.Zuberek, Faculty of Earth Sciences, Silesian University, Sosnowiec–Zawiercie (in Polish) 2010.

[24] Golebiowski T., Tomecka-Suchon T., *GPR Fractures Detection Using Changeable Antennae Orientation*, 5th International Conference and Exhibition, EAEG Org., St. Petersburg 2012.

[25] Annan A.P., *Ground Penetrating Radar*, Workshop Notes, Sensor and Software Inc., Canada 2001.